J. Fluid Mech. (1970), *vol.* 42, *part* 2, *pp.* 269–288
Printed in Great Britain

The laminar flow of dilute polymer solutions around circular cylinders

By DAVID F. JAMES
University of Toronto, Toronto, Ontario, Canada
AND ALLAN J. ACOSTA
California Institute of Technology, Pasadena, California

(Received 23 July 1969 and in revised form 31 December 1969)

This paper describes the measurements of heat transfer and drag for the flow of dilute polymer solutions around very small cylinders. The thermal experiments were carried out at Reynolds numbers less than 50, and the results establish the dependence of the heat transfer on fluid velocity, cylinder diameter, solution concentration, and polymer molecular weight. The drag measurements were conducted with the same type of solutions and in the same Reynolds-number range. To complement the heat-transfer and drag measurements, the flows around a cylinder and through an orifice were examined visually. These flow-visualization studies showed that the streamline pattern with dilute polymer solutions can be significantly different from that with Newtonian fluids because of viscoelastic effects.

An analysis of Rouse's theory of macromolecules shows that for low accelerations a dilute polymer solution behaves mechanically like a Maxwell model. The analysis thereby produces a relaxation time, a single parameter representing the elasticity of the fluid, which can be related to the properties of the solute and solvent. This relaxation time is contained in a new dimensionless group which governs dynamic similarity when induced elastic stresses dominate viscous stresses in the flow around a circular cylinder. The dimensionless group is shown to correlate the thermal data when the heat transfer does not depend on the free stream velocity.

1. Introduction

The recent interest in the fluid mechanics of dilute polymer solutions has been motivated by a phenomenon known as the Tom's effect—the reduction of wall shear stress in a turbulent flow when minute amounts of a high molecular weight polymer are present. The explanation of this effect has been sought in turbulent flow experiments where the parameters associated with drag reduction have been varied. Many long-chain polymers, with different chemical structures and varying molecular weights, have been studied for their effects on turbulent boundary layers, stability and transition. While extensive work has been carried out in the turbulent régime, relatively little attention has been focused on laminar flow. Simple laminar viscometric flows of dilute polymer solutions do not indicate

any unusual flow patterns other than that due to the solution viscosity being slightly greater than the solvent viscosity. Yet experimental difficulties with Pitot tubes and hot wires (Fabula 1966; Smith *et al.* 1967) have suggested that laminar flows with appreciable convective acceleration, such as around blunt bodies, are affected by the dissolved long-chain molecules. In fact, the work to be presented was an outgrowth of the difficulty in using hot-film probes to measure mean and fluctuating velocities in polymer solutions. Instead of trying to cope with the probes' insensitivity and pursuing the original programme, we considered the altered heat loss characteristics to be a significant phenomenon in themselves, and examined them in detail. More than being concerned with the change in heat loss, we directed the investigation to the broader field of the laminar flow around circular cylinders, including drag measurements and flow-visualization studies. We expect that such studies of laminar flows will lead to a better understanding of the dynamic behaviour of dilute polymer solutions, thus contributing perhaps to the eventual explanation of drag reduction in turbulent flows.

2. The polymer solutions

The several experiments reported in this paper were conducted with solutions of a single polymer, and it is perhaps appropriate to provide details of the fluids before describing the experimental hardware. The solute for the aqueous solutions was polyethylene oxide (PEO), a linear polymer available in several molecular weights. A single molecule of this polymer in a stationary solvent is said to be 'randomly-coiled'; that is, the molecular chain assumes a random-walk configuration throughout the solvent. If a number of such macromolecules are present, but the concentration is such that physical interaction is negligible, then the solution is termed dilute. The range of concentrations for the present heat-transfer and drag experiments were within the dilute régime; the lowest concentration was that which produced deviations from the data with pure water, and the maximum was the critical concentration, as defined by Shin (1965).

Polyethylene oxide is commercially available as Polyox,† and three grades of the polymer—WSR-205, WSR-301 and Coagulant—were used directly as received. These industrial blends had unknown distributions of molecular weight but an estimate of the average molecular weight of each blend was found by determining its intrinsic viscosity. With the molecular weight known from light-scattering techniques, Shin found the relation between the intrinsic viscosity $[\eta]$ and the weight-averaged molecular weight $\bar{M}_w$ for Polyox to be

$$[\eta] = 1{\cdot}03 \times 10^{-4} \bar{M}_w^{0{\cdot}78} \quad \text{at } 25\,^{\circ}\text{C},$$

where the intrinsic viscosity is defined as

$$[\eta] = \lim_{c \to 0} \frac{\mu - \mu_s}{c\mu_s},$$

μ = viscosity of solution, μ_s = viscosity of solvent and c = concentration of solute, usually in g/100 ml. The intrinsic viscosity is a measure of the hydro-

† Union Carbide Company.

dynamic influence of the dissolved macromolecules on the flow of the solvent; it is experimentally determined by measuring $(\mu - \mu_s)/c\mu_s$ at various concentrations and extrapolating to $c = 0$. The solutions used to determine $[\eta]$ for each Polyox blend were sampled from the working fluids in the heat-transfer and drag experiments. The solution viscosities were measured in a calibrated, size 50, Cannon–Fenske viscometer. The viscosity measurements could be reproduced to $\pm 0{\cdot}1\,\%$, but repeated intrinsic viscosity analyses of a given solute indicated that $[\eta]$ could be determined only to $\pm 3\,\%$.

Since the polymer solutions used in the heat-transfer investigations were contained in an open tank for up to 2 weeks, we were concerned about the possibility of polymer degradation. Accordingly, the intrinsic viscosity of the WSR-301 solutions in the tank was checked repeatedly over a period of 14 days, and the change in $[\eta]$ was only slightly greater than the $\pm 3\,\%$ experimental accuracy. It was concluded that the molecular weight had not changed appreciably and consequently that degradation did not significantly affect the present work.

3. Heat-transfer experiments

(i) *Description of apparatus and technique*

The experimental apparatus for the measurement of heat transfer from small circular cylinders was essentially the conventional equipment of hot-film anemometry, and the experimental technique was similar to the standard procedure for calibrating hot-film sensors with the use of a tow tank. The cylindrical sensors were towed at known velocities through a variety of polymer solutions while an anemometer and its auxiliary equipment monitored the heat loss.

This section will provide a brief description of the equipment and technique, the complete details for which can be found in James' thesis (1967). The anemometer, a constant-temperature type, was a modification of Shapiro and Edwards Model 60 B, and was originally built for low velocity measurements in water. The anemometer output terminal was connected to an electronic device which squared the current through the sensor, thus facilitating a direct measurement proportional to the dissipated electrical energy, i.e. to the heat loss from the sensor. The connecting cable, probe and hot-film sensors were the standard commercial products of Thermo-Systems Inc. For ordinary velocity measurements a knowledge of the sensor's construction and properties is not necessary; however, these details must be examined when the sensor is employed as a heated, thin-walled tube in heat-transfer experiments.

Three sizes of sensors were available in nominal diameters of 0·001, 0·002 and 0·006 in.; the length-to-diameter ratio varied with each sensor, and ranged from 12:1 to 22:1 for the present sensors. A custom-made 0·006 in. sensor with a much larger ratio of 96:1 was used to check end-effects in both free and forced convection.

The somewhat involved construction of a typical sensor is shown in figure 1. From the drawing, it is evident that the total electrical resistance of the sensor, as measured between the terminals of the sensor holder, is comprised of the resistance of the metallic legs and the resistance of the portion of the platinum

film not overlaid by gold. The resistance of the gold plating and bonding is considered negligible because of gold's high conductivity, and because the gold thickness, 2×10^{-4} in., is much larger than the platinum film thickness of 5×10^{-6} in. Thus the electrical resistance of the 'heated length' in figure 1 was determined by measuring the total sensor resistance and subtracting the estimated resistance—usually 6% of the total—of the metallic legs. The temperature coefficient of resistivity for each hot-film sensor was determined prior to its use in the heat-transfer experiments by measuring its resistance in water at various temperatures. The diameter and the heated length of each sensor were measured by microscopic methods.

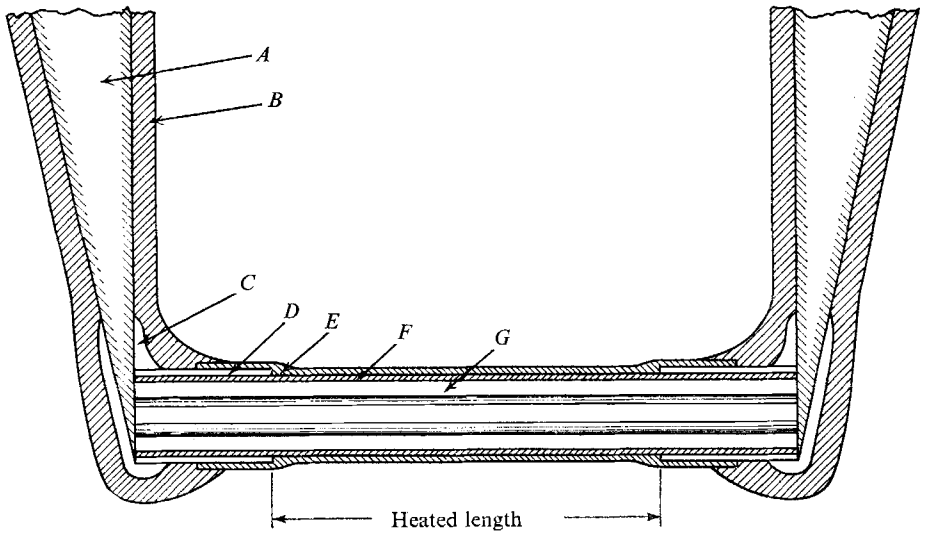

FIGURE 1. A sketch, not to scale, of the construction of a cylindrical hot-film sensor: *A*, Metallic leg of sensor holder (also acts as an electrical terminal); *B*, epoxy coating; *C*, gold bonding for mechanical and electrical connexions; *D*, electroplated gold layer, about 0·0002 in. thick; *E*, vacuum-deposited quartz coating, about 12,000 Å thick, for preventing electrical paths in the external, conducting liquid; *F*, platinum film, about 1000 Å thick; *G*, glass tube. The values for the various thicknesses were supplied by the manufacturer, Thermo-Systems Inc.

The temperature difference maintained between the sensor and the ambient fluid depended on the polymer concentration and on the sensor size. In general a low-temperature difference, of the order of 25 °F, was maintained to avoid difficulties with air bubbles; that is, air dissolved in the aqueous solutions formed bubbles on the surface of the heated cylinder, thereby reducing the heat transfer. When this problem arose, the bubbles were removed by carefully brushing the sensor. With low-temperature differences it was found that the anemometer was not able to maintain the sensor at a constant temperature, but rather allowed it to deviate in a systematic way. A calibration of the anemometer was consequently necessary, and the method and results of this correction procedure can be found in James (1967).

The towing facility, originally constructed for calibration purposes, had a

maximum run of 6 ft. and provided uniform carriage velocities between 0·01 and 1·0 ft./sec. The first experiments were a study of the effect of polymer additives on heat-transfer by natural convection. Three sensors of each size, plus the extra-long sensor, were immersed in distilled water and in solutions of WSR-301, ranging in concentration from 10 to 304 ppmw (parts per million by weight). Energy-dissipation data were recorded for temperature differences between 9 and 84 °F.

The initial measurements of heat transfer by combined forced and free convection were in distilled water; these data served to check the present experimental technique and provided a base for comparing the results with polymer solutions. Heat-transfer data were recorded for the three sizes of sensors in various concentrations of the three grades of polyethylene oxide. For each grade, the first data recorded were for the maximum concentration, and additional data for successively lower concentrations were obtained by continually diluting the original solution.

(ii) *Results*

The measurements of heat transfer by free convection in WSR-301, for concentrations up to 304 ppmw, showed no change from the pure-water data. This result is shown in figure 2 for the three standard sensors; the data with the extra-

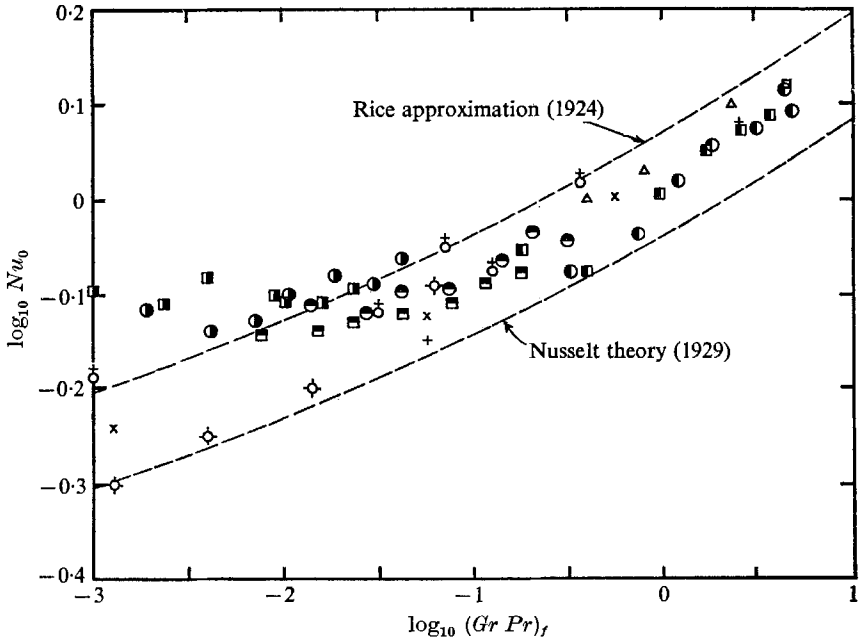

FIGURE 2. Heat transfer by free convection from horizontal circular cylinders. The subscript f indicates that the fluid properties were evaluated at the mean film temperature, the arithmetic average of the surface and ambient temperatures. The round and square symbols respectively represent data in distilled water and in 304 ppmw of WSR-301. ◐, ◧, data with 0·0063 in. cylinder, $L/D = 13$; temperature difference ranged from 4° to 42 °C. ◓, ◨, 0·0021 in. cylinder, $L/D = 18$; ΔT ranged from 5° to 48 °C. ◑, ◨, 0·0011 in. cylinder, $L/D = 14$; ΔT ranged from 5° to 44 °C. The undesignated symbols, representing data of previous investigators, and the two dashed lines are copied from figure 7-10 of McAdams (1954).

long 0·006 in. sensor are not shown here since they coincided with those of the corresponding, shorter sensor. The data for the graph required the computation of the Nusselt number, $Nu = (I^2R)/(\pi kL\Delta T)$, the Grash of number, $Gr = (\rho^2\beta\Delta T D^3)/\mu^2$, and the Prandtl number, $Pr = (C_p\mu)/k$. The direct measurements for I, R, L, D, ΔT and μ have been substituted in the above dimensionless parameters, where I = current through the sensor, R = resistance of the heated length L of the sensor, D = diameter of sensor, ΔT = temperature difference between sensor and fluid, and μ = viscosity. The pure-water values have been used for the specific heat C_p, density ρ, thermal conductivity k, and the thermal expansion coefficient β. No information is available relating C_p, k and β to concentrations of PEO; consequently it was assumed that the changes in C_p, k and β are of the same order as the change in the density. Since the maximum polymer concentration was only 0·3 %, the solvent values for C_p, k, β, and ρ have been substituted. Following standard practice, these properties have been evaluated at the mean film temperature.

To check on the acceptability of the present experimental results for combined free and forced convection, our data with distilled water were compared to those of Davis (1924) and Piret, James & Stacey (1947). Davis measured the heat loss from vertical wires in water and oils, and his results were correlated by the equation

$$\frac{Nu}{Pr^{0\cdot31}} = 0\cdot91\,Re^{0\cdot395} \quad (0\cdot1 < Re < 50).$$

Piret conducted similar experiments in water but with horizontal wires, and found the parameters related by

$$\frac{Nu}{Pr^{0\cdot30}} = 0\cdot965\,Re^{0\cdot28} \quad (0\cdot08 < Re < 8).$$

Our data in distilled water with three standard sensors, positioned horizontally, agreed with these previous investigations. As an example, the results with the 0·002 in. sensor are plotted in figure 3 along with the above two equations.

The heat-transfer results in polymer solutions are presented in figures 4–6, and these represent the bulk of the experimental work. In each graph the Nusselt number is plotted as a function of the Reynolds number, and each graph includes the data for one molecular weight. The three sets of data contained in each figure correspond to the results for the three cylinder sizes.

An auxiliary test with the extra-long 0·006 in. sensor in a typical polymer solution produced forced convection data similar to those with a standard 0·006 in. sensor. It was concluded that the sensors were long enough that the flow pattern about them could be considered two-dimensional.

4. Drag experiments

A comparison of the heat-transfer results between water and various polymer solutions suggested that the velocity field about the circular cylinder was significantly different when dissolved macromolecules were present. To gain additional information about the nature of the flow field, an experimental in-

vestigation was undertaken to measure the drag on a very small cylinder at the same Reynolds numbers and polymer concentrations as in the heat-transfer studies.

The drag was measured by immersing a portion of a vertical wire, fixed at the top end only, into a rotating basin of liquid and monitoring the force by measuring the deflexion of the free end. A sketch of the apparatus for this experiment is shown as figure 7. The deflexions of the cantilever wire were as small as 10^{-3} in., and consequently were measured with a travelling-stage microscope coupled

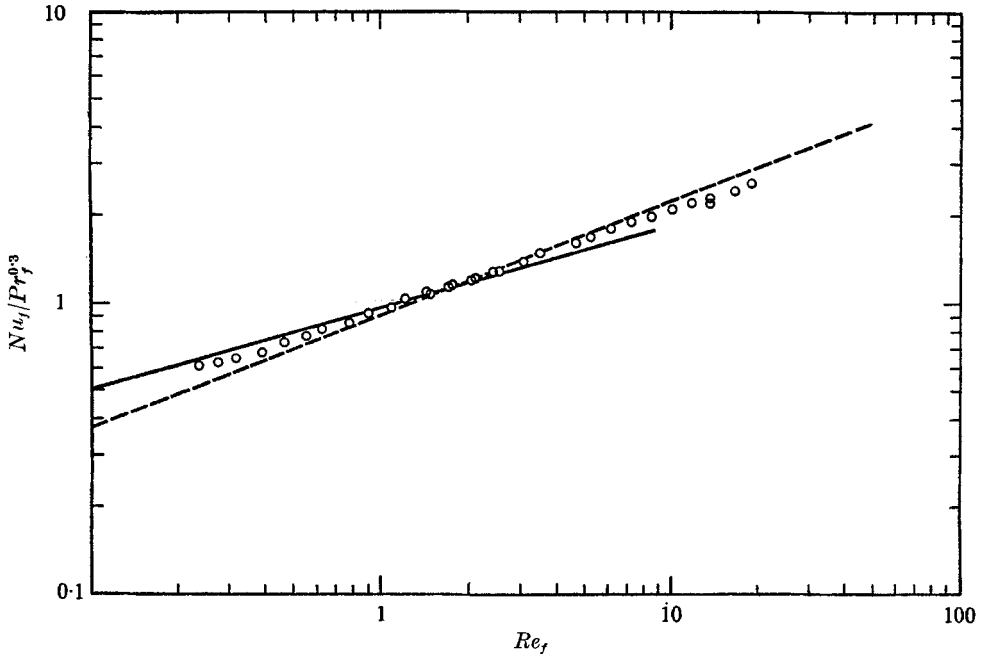

FIGURE 3. A comparison of our data in distilled water with those of previous investigators in Newtonian fluids for heat transfer from circular cylinders by combined free and forced convection. The present data were obtained with a 0·0021 in. cylinder having a length-to-diameter ratio of 18:3; the temperature difference was 12·4 °C. The data by Piret *et al.* and Davis were for horizontal and vertical wires respectively. The subscript f again denotes that fluid properties were evaluated at the mean film temperature. ○, present data for water; ——, correlation of data by Piret *et al.* (1947); – – –, correlation of Davis's (1924) data.

with a micrometer accurate to $\pm 0{\cdot}0001$ in. The optical distortion due to the curvature of the tank wall was taken into account by comparing the stage micrometer readings with known distances at the focal plane through the wire. The microscope was supported on an elevator table so that the wire, which sometimes caught minute fibres suspended in the fluid, could be viewed along the length of the immersed portion. The cantilever wire was hand-straightened music wire of 0·0050 in. diameter, and usually about 1·5 in. was immersed in the liquid, providing a submerged length-to-diameter ratio of 300:1. To prevent rust, an epoxy coating was baked on the wire, increasing its diameter by 0·0002 in. A

fixed-end condition at the top of the wire was ensured by freezing it in a type of Woods metal.

The computations relating the wire deflexion to the fluid drag force required the value of the flexural rigidity of the wire. This parameter, usually denoted EI, was determined by supporting the wire horizontally, placing known weights at known locations, and measuring the deflexions to 0·0001 in. with an optical comparator. The resulting data indicated that, within the experimental accuracy of $\pm 1\,\%$, the load–deflexion relationship was linear for deflexions less than 6 % of the wire length.

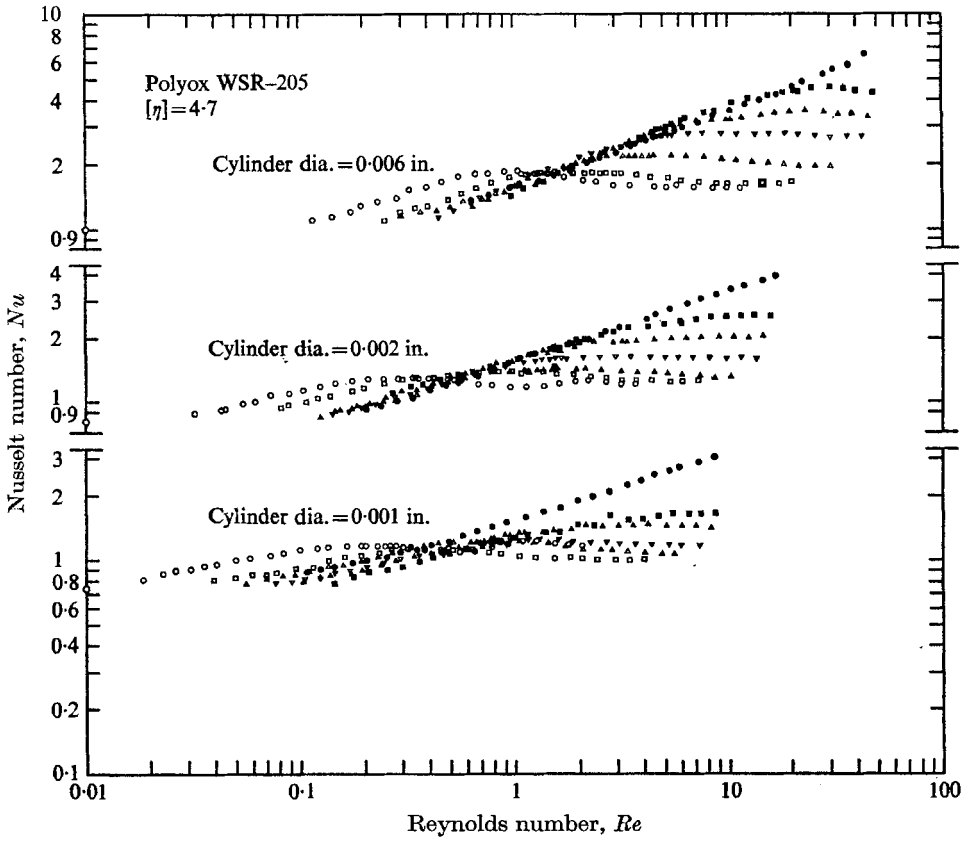

FIGURE 4. Heat transfer by combined free and forced convection from small cylinders in solutions of WSR-205, $[\eta] = 4{\cdot}7$. ●, distilled water; ■, 101 ppmw; ▲, 206 ppmw; ▽, 383 ppmw; △, 740 ppmw; □, 1460 ppmw; ○, 3010 ppmw. Symbol at left-hand edge, ○, represents free convection data ($Re = 0$).

Six solutions of WSR-301 were prepared for the drag measurements. Similar to the heat-transfer measurements, the concentrations of the working solutions increased in geometric progression, and the maximum concentration roughly equalled the critical concentration for the particular molecular weight. Each solution was prepared by mixing a known portion from a master solution with fresh distilled water.

To check on the uniformity of the velocity profile in the tank, small potassium permanganate crystals were dropped into the rotating liquid. At steady-state conditions, the vertical dye streaks were straight except for a distortion near the free surface due to air drag. Measurements of the distortion showed that the error in assuming a uniform velocity profile was negligible. When the fluid speed at the wire was less than 0·4 ft./sec, it was found that the deflexion measurements were reproducible to within 0·0001 in. At higher velocities up to 1·0 ft./sec, this error increased to as much as 0·005 in. because of vibrations of the wire; this motion was apparently due to the unsteadiness of the wake behind the cylinder,

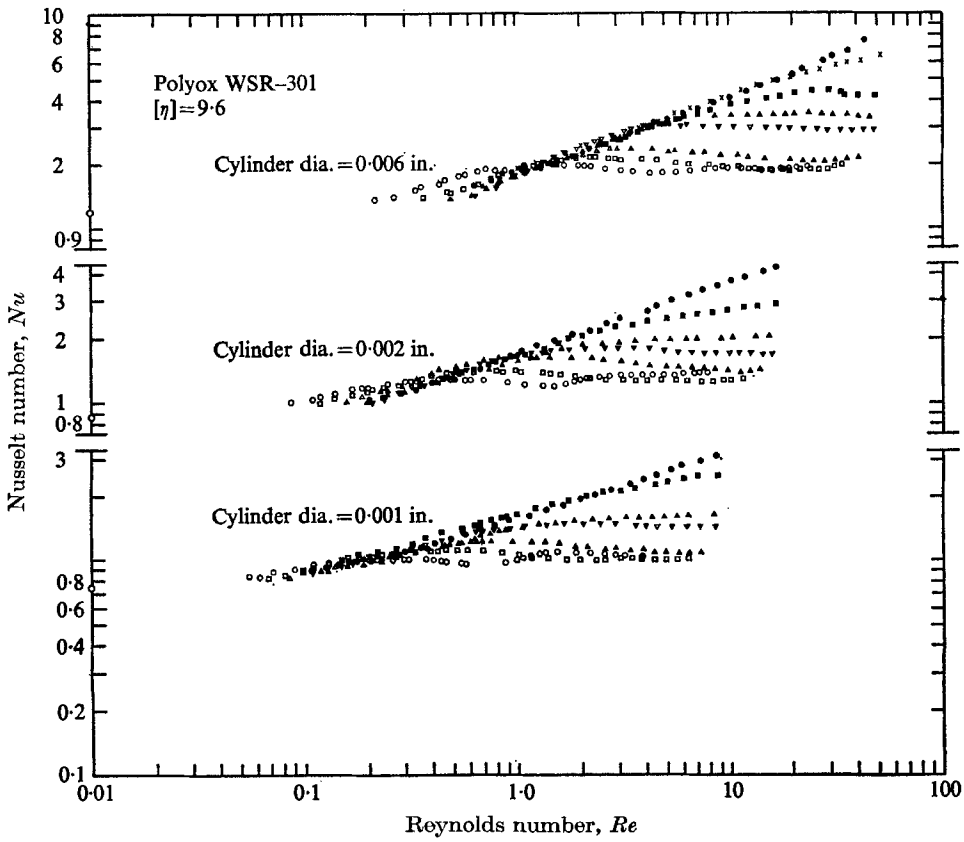

FIGURE 5. Heat transfer by combined free and forced convection from small cylinders in solutions of WSR-310, $[\eta] = 9{\cdot}6$. ●, distilled water; ×, 6·62 ppmw; ■, 13·2 ppmw; ▲, 26·2 ppmw; ▽, 52·4 ppmw; △, 102 ppmw; □, 205 ppmw; ○, 404 ppmw. Symbol at left-hand edge, ○, represents free convection data ($Re = 0$).

an expected behaviour when the Reynolds number is greater than 30 (Van Dyke 1964).

The results of the drag measurements for distilled water and six polymer solutions are shown in figure 8. The data are plotted in the usual form of the drag coefficient C_D *versus* the Reynolds number Re, and the graph includes the classic data of Wieselsberger (1923) for Newtonian fluids. The computations for

C_D were based on the assumption that the cantilever wire was uniformly loaded along a portion of its length; the relation between the uniform load and the deflexion of the free end is readily found from bending-beam analysis.

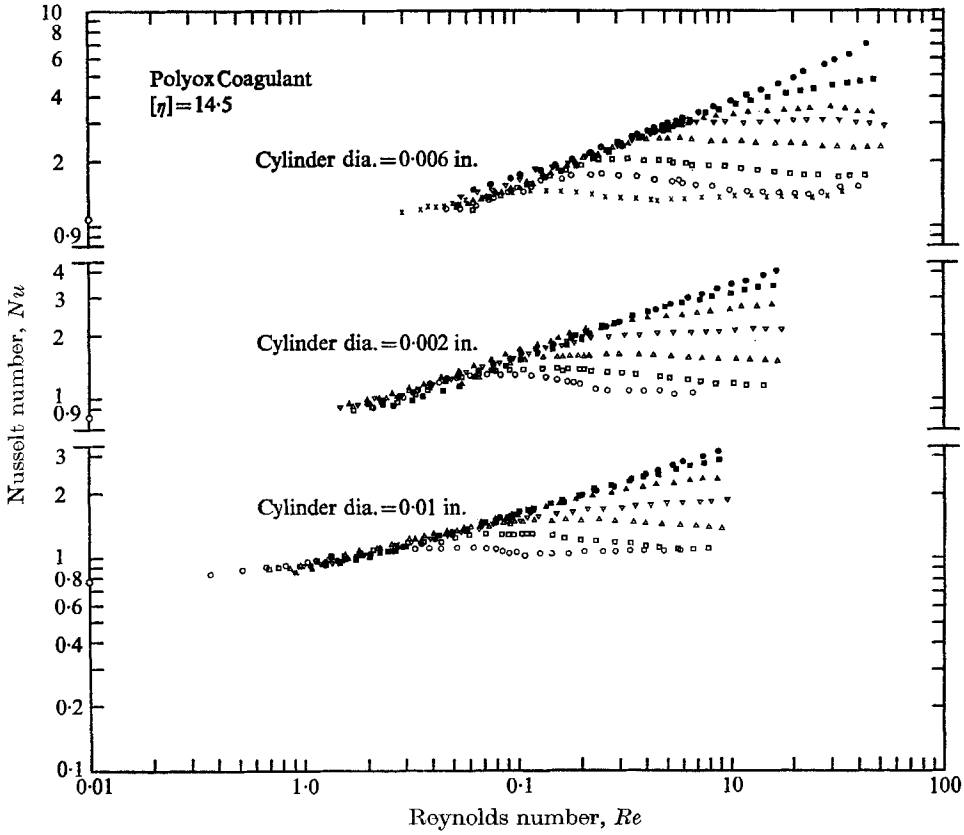

FIGURE 6. Heat transfer by combined free and forced convection from small cylinders in solutions of Coagulant, $[\eta]$ = 14·5. ●, distilled water; ■, 4·18 ppmw; ▲, 6·68 ppmw; ▽, 11·3 ppmw; △, 20·3 ppmw; □, 38·4 ppmw; ○, 78 ppmw; ×, 153 ppmw. Symbol at left-hand edge, ○, represents free convection data (Re = 0).

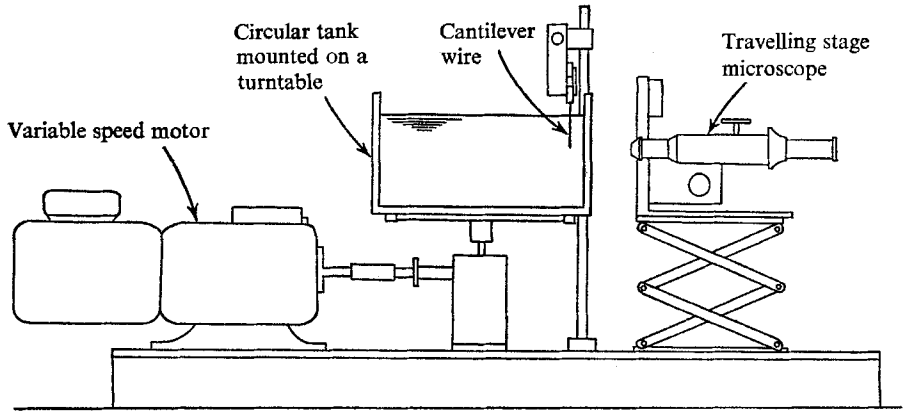

FIGURE 7. Experimental set-up for measuring the drag on a small circular cylinder.

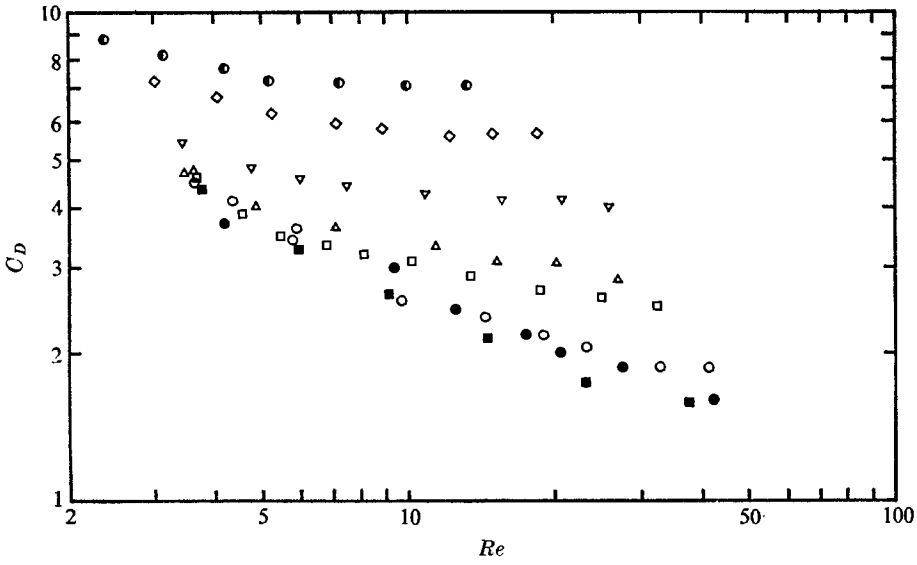

FIGURE 8. Drag force on a 0·005 in. wire in water and in solutions of WSR-301, $[\eta] = 15$. ●, Wieselsberger's data (1923); ■, present data for distilled water; ○, 7·4 ppmw; □, 15·7 ppmw; △, 30 ppmw; ▽, 60 ppmw; ◇, 119 ppmw; ◐ 226 ppmw.

5. Flow visualization around a circular cylinder

The speculation that the flow field around a circular cylinder was different in polymer solutions led us to set up dye-injection equipment to visualize the streamlines. Again a variable-speed rotating table was used, as in the drag experiments, but this time with a transparent tank bottom so that the 0·005 in. wire could be seen end-on from below. By using several prisms and lenses the object was viewed in a standard upright microscope situated outside the tank. The dye-injection apparatus consisted of four stainless-steel tubes (I.D. = 0·006 in., O.D. = 0·013 in.), each 3 in. long and attached 0·5 in. apart to a header located above the liquid. The tubes were bent so that they smoothly converged and various configurations were tried until the disturbance to the flow was a minimum. Even with care, however, it was not possible to eliminate completely the slight convergence of the streaklines in the wake of the injection tubes. For water, the centre-to-centre distance at the tube ends was 0·020 to 0·025 in., while much larger distances were necessary in the polymer solutions. The dye used in this study was lamp black in water; this apparently does not react quickly with Polyox since fluid samples from the tank had the same viscosity before and after the addition of dye. Flow patterns around the immersed cylinder were observed and photographed for several velocities and with three fluids: water, and 30 ppmw and 60 ppmw of Polyox Coagulant. The results are shown in the 12 photographs of figure 9 (plates 1 and 2).

6. Flow pattern of a minute laminar jet

The differences in the heat-transfer and drag data between water and dilute polymer solutions were thought perhaps to be a result of normal stress effects. Standard techniques have been developed for measuring these stresses in viscoelastic fluids (Coleman, Markovitz & Noll 1966; Lodge 1964), but invariably the liquids tested have been concentrated polymer solutions. Apparently no measurements have been reported to indicate the magnitude of the stresses for dilute solutions. A simple visual appreciation of this magnitude was provided by the

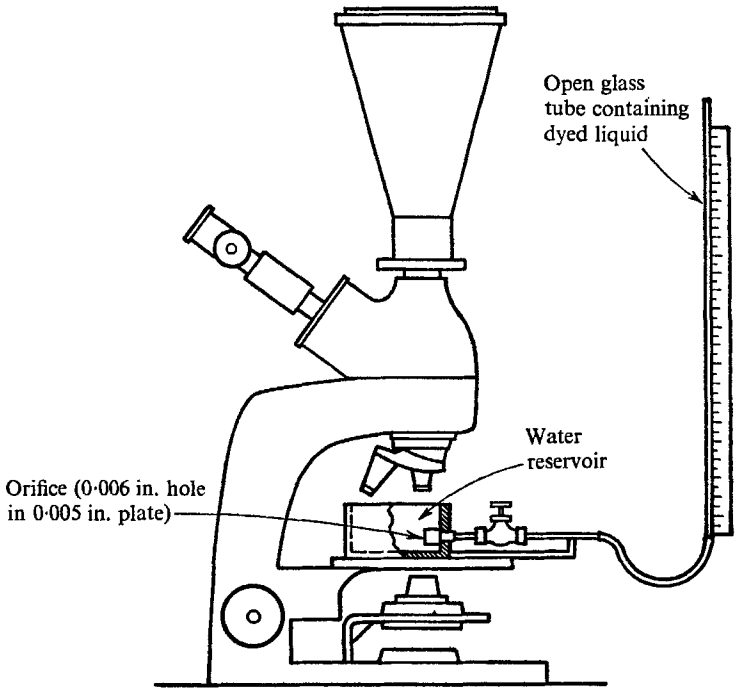

FIGURE 10. Apparatus for examining the laminar jet issuing from a minute orifice into a water reservoir.

flow pattern of a minute laminar jet. This particular flow geometry was patterned after the well-known 'die-swell' effect for streams of concentrated solutions (see e.g. Lodge, p. 242). The flow parameters for the small circular jets were selected to duplicate the Reynolds number and fluid acceleration of the submerged cylinder flows.

Figure 10 shows the arrangement of the equipment for the visual studies. The microscope was focused on the fluid issuing into a clear water reservoir through a 0·0064 in. diameter hole drilled in a 0·005 in. thick plate. The orifice plate was cemented to the end of $\frac{1}{8}$ in. Polyflo tubing connected to an open vertical tube. Black aniline dye was dissolved in the issuing liquid to make the jet outline visible; the dye increased the fluid viscosity by approximately 5 %. The black aniline dye reacted slowly with the PEO solute, but was still found suitable for gross effects when used immediately after mixing with a polymer solution.

Photographs were taken of water and a nominal 87 ppmw solution of WSR-301 issuing from the orifice at mean velocities between 0·2 and 2·5 ft./sec. At low velocities the water jet was undulatory and diverged at a considerable angle as shown in figure 11 (*a*) (plate 3); with increasing velocity, the divergence angle decreased to a very small value, illustrated in figure 11 (*b*) for $V = 1{\cdot}5$ ft./sec. When the issuing fluid was the polymer solution, the flow pattern was similar to that for water when the velocity was less than about 0·4 ft./sec. At higher flow rates the jet enlarged immediately upon issuing from the orifice. Figure 11 (*c*), which was photographed at the same magnification as figures (*a*) and (*b*), shows that the jet swelled to about four times the orifice diameter at a velocity of 1·0 ft./sec

A similar study was conducted with a $\frac{1}{2}$ in. hypodermic needle having an inside diameter of 0·0062 in. The end of the needle was ground flat and deburred. Circular jets into water were again observed for water and a nominal 83 ppmw solution at mean velocities between 0·1 and 2·5 ft./sec. At low speeds the jet shapes of solvent and solution were identical. At higher speeds the water jet diverged at a very small angle while the solution jet expanded to a diameter of 0·012 in.

The jet swell shown in the photographs is similar to the 'die-swell' effect for concentrated solutions. The flow pattern in both cases is due to the elasticity of the fluid, that is, to normal stress effects. Even though the polymer solutions for the laminar jet were not well characterized due to the dye-solute reaction, the photographs clearly indicate that normal stress effects can be very significant even for dilute solutions.

7. Discussion of the experimental results

The heat-transfer and drag data, supported by the flow-visualization studies, indicate that minute amounts of a high weight polymer can significantly affect a laminar flow subject to convective acceleration. Previous experimental work on polymer solutions has focused primarily on the turbulent régime where the solute produces considerable drag reduction in shear flows. We note that the gross effects in laminar and turbulent flow are of the same order. Investigations of turbulent pipe flow have reported drag reduction by as much as 80 % (Hoyt & Fabula 1964). In comparison, the present measurements in laminar flow show that, at the highest Reynolds number tested, the heat loss from cylinders is reduced by at least 70 % and that the drag on a cylinder can be increased by a factor of three.

The general pattern of cylinder heat transfer in dilute polymer solutions at Reynolds numbers below 50 is shown in figures 4–6. At low velocities, the heat loss is identical to that for water; but at some critical speed the heat-transfer data for a given concentration depart from the pure-water data, and in many cases become independent of the flow velocity. The juncture of the water data with the data of a particular solution will be termed the critical Reynolds number Re_c, and the three graphs demonstrate that Re_c decreases as the cylinder diameter decreases, and as the polymer concentration and molecular weight increase. A similar dependence of Re_c on the solution concentration isalso evident in the

drag measurements. Table 1 compares the Re_c values from the drag measurements with those from the thermal data at similar flow conditions. Considering the accuracy in determining Re_c from the experimental data, the two sets of Re_c values are reasonably similar, and establish that a change in the flow pattern occurs at some critical condition which affects both heat transfer and drag. Unfortunately, further comparisons are not possible from the present data because of the single polymer grade, single cylinder size, and limited velocity range in the drag measurements.

Polymer concentration (ppmw)	Re_c from drag measurements (figure 8) $[\eta] = 15$, $D = 0{\cdot}005$ in.	Interpolated Re_c from heat-transfer data (figure 6) $[\eta] = 14{\cdot}5$, $D = 0{\cdot}006$ in.
7·4	10	6
15·7	7	4·5
30·2	3·5	3

TABLE 1

The reduced heat transfer and increased drag appear to be due to viscoelastic effects. Fabula (1966) suggested that the long molecular chains coat the small wires, but the flow-visualization studies demonstrate that the flow pattern is altered because of the liquid's elasticity. This fluid property appears most evident in the photographs of the minute laminar jet. Upon issuing from the orifice, the jet diameter increased by as much as four times its initial value. Since jet swelling is a qualitative measure of the liquid elasticity (Coleman *et al.* 1966), it is evident that the induced axial stresses are negative and have considerable effect even for dilute solutions. Since the fluid velocity and acceleration for the laminar jets were comparable to those for cylinder flows, it may be expected that viscoelasticity should also affect the streamline pattern for the flow around a submerged cylinder. Indeed, such is the case, as shown by the photographs of figure 9. It is evident that the region of the flow field influenced by the cylinder is much greater in polymer solutions than in water alone, and that the effect is more pronounced at higher speeds and higher concentrations, concomitant with the experimental data. The most noticeable differences in the flow pattern are the upstream influence of the cylinder, and the increased width of the wake. It appears that the region disturbed by the cylinder can be an order of magnitude larger with polymer solutions than that with Newtonian fluids. The behaviour at the leading edge supports the hypothesis which Metzner & Astarita (1967) proposed to explain our heat-transfer data, which was made available to them some time ago. They suggested that the boundary layer around a small blunt object, such as a cylinder or wedge, was thickened because of the large deformation rate of the elastic liquid. While Metzner & Astarita were mainly concerned with the distortion of the flow close to the stagnation point, the photographs demonstrate that for cylinder flows equally important changes take place in the neighbourhood of the separation points and in the wake.

As noted, the stretching of the flow field readily explains the reduction of heat transferred: the velocity gradients at the wall are diminished, thereby reducing

the thermal convection. In contrast, the drag results cannot be explained directly by the streamline pattern; in fact, the lower velocity gradient at the front of the cylinder reduces the viscous component of the drag. To account for the increased drag, the pressure distribution around the cylinder must vary appreciably from that for a Newtonian fluid. The altered pressure distribution, a result of normal stress effects, is quite obvious from the photographs, which show an outward 'stretching' of the flow field. An estimate of normal stress effects on the pressure distribution cannot be made directly since no measurements of the normal stresses are available for dilute solutions. However, an order of magnitude calculation of the normal stress differences can be made from the laminar jet photographs. A momentum balance shows that the axial pressure difference, between points just inside and outside the orifice, is of the order ρV^2 for the situation when the jet diameter is much larger than the orifice diameter. For cylinder flows this suggests that the differences in the pressure distribution due to normal stress effects are $O(\rho V^2)$. Thus we would expect the drag coefficient C_D to be changed by $O(\Delta P/(\frac{1}{2}\rho V^2))$, i.e. by $O(1)$. This, indeed, appears to be the case as shown by the drag data.

8. Correlation of the heat-transfer data

We now seek to correlate the heat-transfer data in the régime where the Nusselt number is virtually independent of the Reynolds number. Figures 4–6 indicate that with most of the solutions tested the heat transfer approaches a maximum value at high velocities, or at most is a very weak function of the Reynolds number. In this region the Nusselt number is determined by the cylinder diameter and by the polymer concentration and molecular weight. We desire to combine these variables into a dimensionless group which will correlate the experimental data. The first stage in formulating this dimensionless group is the derivation of a fluid relaxation time from the theory of the mechanical behaviour of macromolecules; this parameter is then combined with other flow variables to form the desired dimensionless group.

(i) *A relaxation time for dilute polymer solutions*

Density and viscosity are well defined and readily measurable properties of most fluids. Polymer solutions have the additional property of elasticity, and its magnitude is usually found from measurements of normal stresses. However, the standard techniques have not been able to provide values for dilute polymer solutions because of the sensitivity required in measurement. Lacking experimental information, we propose to use a quantity, derived from the theory of macromolecules, to represent the elasticity of the solution. The derivation is based on the work of Rouse (1953), and will show that when a dilute polymer solution is subjected to oscillatory shear at low frequencies, the dynamic behaviour of the fluid corresponds approximately to that of the Maxwell model, namely a spring and dashpot in series. The elasticity in this simple mechanical model can be expressed in a single parameter, the relaxation time, and the analysis to follow will relate this quantity to the properties of solute and solvent.

The fundamental work on the mechanical behaviour of dilute polymer solutions is due to Rouse (1953). He analyzed the response of discrete long-chain molecules in an oscillatory shear flow, and found that the molecular motion depended on a series of relaxation times.

$$\tau_p = \frac{6M[\eta]\eta_s}{\pi^2 p^2 RT} \quad (p = 1, 2, 3, \ldots),$$

where M = polymer molecular weight, $[\eta]$ = intrinsic viscosity, η_s = viscosity of the solvent, R = gas constant, and T = temperature (η, and not μ, will be the symbol for viscosity in this section of the work, in order to follow the notation of Rouse). The τ_p are essentially a measure of the time required for a macromolecule to return to its equilibrium configuration after an initial distortion. While Rouse's original analysis was a perturbation technique based on small strain rates, Walsh (1967) has since shown that the solution is in fact valid for all strain rates. Rouse's solution can be expressed in terms of the shear stress, which, for the applied shear strain rate $\alpha_0 \cos \omega t$, is as follows:

$$S = \alpha_0\left(\eta_s + \frac{6(\eta_0 - \eta_s)}{\pi^2}\sum_{p=1}^{N}\frac{1}{p^2(1+\omega^2\tau_p^2)}\right)\cos\omega t + \alpha_0\frac{6}{\pi^2}(\eta_0 - \eta_s)\sum_{p=1}^{N}\frac{\tau_p}{p^2(1+\omega^2\tau_p^2)}\omega\sin\omega t,$$

where S = shear stress, ω = frequency, α_0 = strain rate, η_0 = viscosity of solution under steady shear ($\omega = 0$). When the frequency is such that $\omega^2\tau_p^2 \ll 1$, and when the substitution is made τ_p, the above expression reduces to

$$S = \alpha_0\left(\eta_s + \frac{6}{\pi^2}(\eta_0 - \eta_s)\sum_{p=1}^{N}\frac{1}{p^2}\right)\cos\omega t + \alpha_0\frac{36}{\pi^2}(\eta_0 - \eta_s)\frac{[\eta]M\eta_s}{RT}\sum_{p=1}^{N}\frac{1}{p^4}\omega\sin\omega t.$$

Since the upper integer N is $O(10^2)$, both summations can be evaluated by replacing N by ∞. Also, $\eta_0 - \eta_s$ is given by

$$\eta_0 - \eta_s = \eta_s[\eta]c(1 + k[\eta]c),$$

where c = concentration of solute, in g/100 ml. Since k is about 0·35 (Tanford 1961), and since $[\eta]c$ is $O(10^{-1})$ for dilute solutions, the second term in the above expression can be neglected. The equation for S then becomes

$$S = \alpha_0\eta_s\left[\frac{\eta_0}{\eta_s}\cos\omega t + \frac{2}{5}\frac{\eta_s[\eta]^2 Mc}{RT}\omega\sin\omega t\right].$$

If the difference between η_0 and η_s can be neglected, being of $O(10^{-1})$ as mentioned, the expression for S may be written as

$$S = \alpha_0\eta_s[\cos\omega t + \tau\omega\sin\omega t],$$

which is equivalent to the low-frequency response of a Maxwell model whose viscosity and relaxation time are η_s (or η_0) and τ respectively. Thus at low frequencies a dilute solution behaves mechanically as a Maxwell model, and the model relaxation time τ is related to the solution properties by

$$\tau = \frac{2}{5}\frac{\eta_s[\eta]^2 Mc}{RT}.$$

It must be noted that τ depends only on the properties of the solute and solvent and not on the frequency or strain rate of the motion. The above expression can be rearranged as

$$\tau = \frac{\pi^2}{15}[\eta]c\tau_1,$$

where τ_1 is the largest relaxation time for the individual macromolecules. In this form, τ is seen to be proportional both to the molecular relaxation time and to the dimensionless concentration $[\eta]c$, a relation which appears quite reasonable on physical grounds.

The parameter τ will be combined with other variables in the next section, but we should first point out that it is similar to a parameter used by Walsh (1967) to correlate turbulent drag reduction. Like the present work, the analysis by Walsh was based on Rouse's solution, but where we sought a fluid relaxation time, Walsh sought to calculate the energy stored by macromolecules in a particular flow, namely in steady shear ($\omega = 0$). By using Rouse's general solution and by integrating the energy distribution of polymer segments over configuration space, Walsh found that the total energy stored was $(\alpha_0^2\eta_s^2[\eta]^2 Mc)/5RT$ (or $\frac{1}{2}(\alpha_0^2\eta_s\tau)$ in our notation), and that this group correlated Shin's (1965) drag-reduction data for circular Couette flow. The same computation of the stored energy can be made more readily using our result that a polymer solution behaves as a Maxwell-type fluid at low frequencies. That is, under a steady shear strain of magnitude α_0, the energy stored in a Maxwell fluid of viscosity η_s and relaxation time τ can easily be shown to be, as expected, $\frac{1}{2}(\alpha_0^2\eta_s\tau)$.

Since we intend to employ τ for correlating data for the flow around a circular cylinder, it is essential to show that the main simplification in the preceding analysis for oscillatory shear flow, i.e. that $\omega^2\tau_p^2 \ll 1$, is appropriate for cylinder flows. The condition that $\omega^2\tau_p^2 \ll 1$ in oscillatory shear is equivalent to specifying that the local acceleration of the fluid is everywhere small. For steady flow past a submerged body, the analogous condition is that the local convective acceleration be small. This condition appears to be satisfied, if we judge by the flow-pattern photographs of figure 9. The photos show that (*a*) the region of the flow field influenced by the cylinder is much larger in a polymer solution than in the solvent, and (*b*) in a polymer solution the region increases as the free stream velocity increases. Thus the fluid acceleration is always small, independent of the external flow. Consequently it appears that τ is an appropriate fluid parameter for flows of polymer solutions around small bodies.

(ii) *Dynamic similarity*

If τ can be considered the fluid property representing elasticity, then in general the heat transferred by convection from a circular cylinder will depend on the flow variables V, D, ρ, μ and τ. The experimental data show that at high velocities the heat-transfer coefficient Nu is virtually independent of V, so that in this régime the functional relationship is reduced to

$$\overline{Nu} = \overline{Nu}(D, \rho, \mu, \tau).$$

The only dimensionless group that can be formed from these four variables is $D^2\rho/\mu\tau$; hence we expect

$$\overline{Nu} = \overline{Nu}(D^2/\nu\tau),$$

and it is in this form that the heat-transfer data have been plotted in figure 12. $\overline{Nu}$ is understood to mean the maximum and/or average value of Nu in the region where Nu is essentially independent of Re, and the values for $\overline{Nu}$ in figure 12 are found from figures 4–6. The parameter τ was calculated for each fluid from the measurements of c, T, μ_s and $[\eta]$; M was computed from $[\eta]$ using Shin's (1965) relationship which was given in the section on polymer solutions. Figure 12 represents data combining three cylinder sizes, three polymer molecular weights, and several concentrations of each molecular weight; the graph indicates a good measure of correlation, there being no discernible pattern in the scatter to suggest that $\overline{Nu}$ depends on D or $[\eta]$ separately.

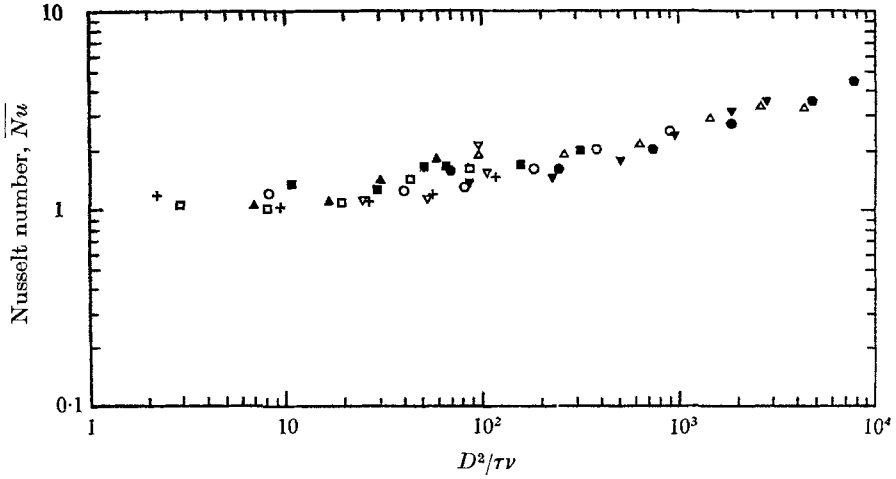

FIGURE 12. The heat-transfer coefficient $\overline{Nu}$ plotted against the similarity parameter $D^2/\tau\nu$. $\overline{Nu}$ is the heat loss from a circular cylinder in the régime where Nu does not depend on the Reynolds number.

Symbol	Cyl. dia. (in.)	$[\eta]$
+	0·001	4·7
○	0·002	4·7
●	0·006	4·7
□	0·001	9·6
■	0·002	9·6
△	0·006	9·6
▲	0·001	14·5
▽	0·002	14·5
▼	0·006	14·5

We had originally thought otherwise, but the grouping, $D^2/\tau\nu$, is not entirely new to the literature on fluid mechanics. For example, Poreh & Paz (1968) introduced a 'polymer number' $\sqrt{(\tau\nu)}/D$ in their analysis to estimate heat transfer in turbulent pipe flow. Using pipe velocity measurements by Elata, Lehrer & Kohanovitz (1966) and the analogy between heat and momentum transfer,

Poreh & Paz predict turbulent heat-transfer rates which depend on the Reynolds number, Prandtl number, and $\sqrt{(\tau\nu)}/D$. In fact, the group $\sqrt{(\tau\nu)}/D$ arises in their paper from a reworking of a dimensionless group proposed by Elata *et al.* to correlate their own velocity measurements. The time τ in the Poreh and Paz parameter is τ_1, the largest molecular relaxation time, and not the fluid relaxation time as in our case. They conducted heat-transfer experiments to check their theory, but unfortunately the chosen polymer was Guar Gum, for which τ_1 cannot be evaluated since the $[\eta]$-$\bar{M}_w$ relationship is not known. Consequently, they were not able to correlate their measurements of heat transfer with computed values of $\sqrt{(\tau_1\nu)}/D$.

Although the parameter $D^2/\tau\nu$ arises naturally from dimensional reasoning, it has considerable physical significance as well. This can be approached most readily by recalling that with a Maxwell model the Weissenberg number $\tau V/D$ is often interpreted as the ratio of elastic forces to viscous forces (see e.g. Metzner, White & Denn 1966). We note that in the present problem $\tau V/D$ also represents the ratio of the fluid relaxation time to the characteristic time of the flow. If the inverse of the Weissenberg number is multiplied by the Reynolds number, the latter being the ratio of inertia to viscous forces, the product is $D^2/\tau\nu$, which then can be interpreted as the ratio of inertia to elastic forces; that is,

$$\frac{D^2}{\tau\nu} = \frac{\text{inertia forces}}{\text{elastic forces}}.$$

In this sense, then, $D^2/\tau\nu$ is the analogue of the Reynolds number when the elastic stresses, and not the viscous stresses, determine the flow field.

Using the above physical interpretation for $D^2/\tau\nu$, the overall physical picture for cylinder flows can be presented in a straightforward manner. At low velocities and consequently at low strain rates, the induced elasticity is small and viscous stresses dominate the flow field. For this situation, which is for small Weissenberg numbers, the fluid behaves as a Newtonian fluid, and the Reynolds number is the appropriate parameter for dynamic similarity. However, at high velocities the strain rates and Weissenberg numbers are large, the elastic stresses dominate the viscous stresses, the flow field is stretched and similarity of the flow field is then governed by the parameter $D^2/\tau\nu$.

As shown in figure 12, the heat-transfer data support the assertion that $D^2/\tau\nu$ is the appropriate similarity parameter. The drag data, which are far less extensive, tend to show the same flow behaviour. Although the tests at the lowest Reynolds numbers were limited, the data indicate Newtonian behaviour for polymer solutions at low velocities. At high velocities the drag coefficient appears to be independent of Re, and it is anticipated that sufficient data would show

$$C_D = C_D(D^2/\tau\nu)$$

in this régime.

This work was supported under the Office of Naval Research Contract N00014-67-A-8094-0012 and by the National Research Council of Canada.

REFERENCES

COLEMAN, B. D., MARKOVITZ, H. & NOLL, W. 1966 *Viscometric Flows of Non-Newtonian Fluids*. New York: Springer.

DAVIS, A. H. 1924 *Phil. Mag.* **47**, 1057.

ELATA, C., LEHRER, J. & KOHANOVITZ, A. 1966 *Israel J. Tech.* **4**, 87.

FABULA, A. G. 1966 Ph.D. thesis, the Pennsylvania State University.

HOYT, J. W. & FABULA, A. G. 1964 *U.S. Naval Ordnance Test Station, China Lake, California, NAVWEPS Report* 8636.

JAMES, D. F. 1967 Ph.D. thesis, California Institute of Technology.

LODGE, A. S. 1964 *Elastic Liquids*. New York: Academic.

MCADAMS, W. H. 1954 *Heat Transmission* (3rd. edn.). New York: McGraw-Hill.

METZNER, A. B., WHITE, J. L. & DENN, M. M. 1966 *A.I.Ch.E. J.* **12**, 863.

METZNER, A. B. & ASTARITA, G. 1967 *A.I.Ch.E. J.* **13**, 550.

PIRET, E. L., JAMES, W. & STACEY, W. 1947 *Ind. Engin. Chem.* **39**, 1098.

POREH, M. & PAZ, U. 1968 *Int. J. Heat Mass Transfer*, **11**, 805.

ROUSE, P. E. 1953 *J. Chem. Phys.* **21**, 1272.

SHIN, H. 1965 Sc.D. thesis, M.I.T.

SMITH, K. A., MERRILL, E. W., MICKLEY, H. S. & VIRK, P. S. 1967 *Chem. Eng. Sci.* **22**, 619.

TANFORD, D. 1961 *Physical Chemistry of Macromolecules*. New York: Wiley.

VAN DYKE, M. 1964 *Perturbation Methods in Fluid Mechanics*. New York: Academic.

WALSH, M. A. 1967 Ph.D. thesis, California Institute of Technology.

WIESELSBERGER, C. 1923 *Ergebn. aerodyn. VersAnstalt zu Göttingen*, II Lieferung, 24.

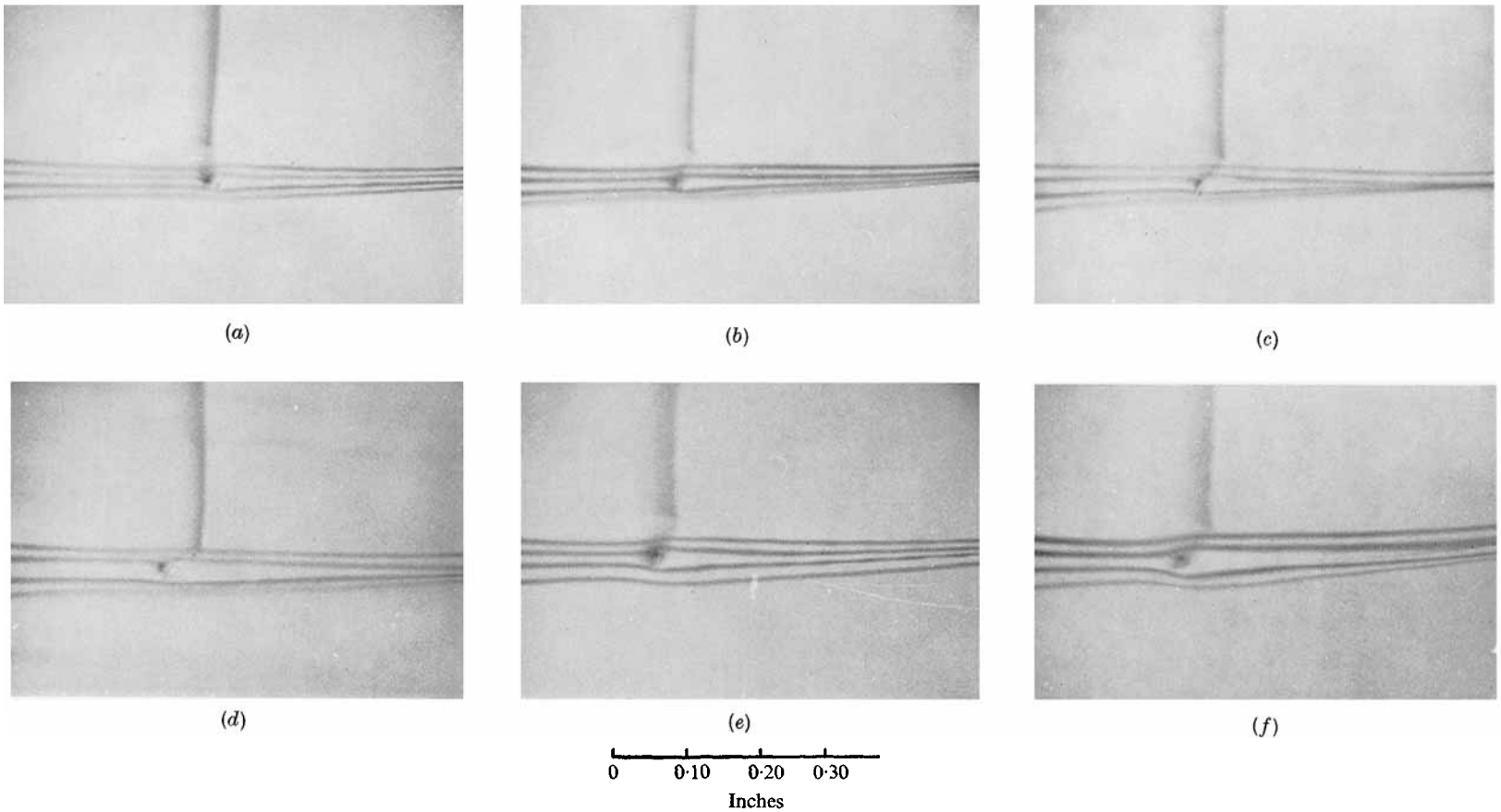

FIGURE 9. Photographs of streaklines showing the disturbance to the flow field caused by a 0·005 in. cylinder in water and in dilute solutions of Polyox Coagulant. The fluid motion here is from left to right, and each photograph is taken at the same magnification. The circular cylinder is viewed end-on and hence is considerably out of focus; the dark spot and line in each photograph are part of the fixture supporting the cantilever wire. The table shown in the second half of figure 9 relates the flow conditions for each photograph.

(*Facing p.* 288)

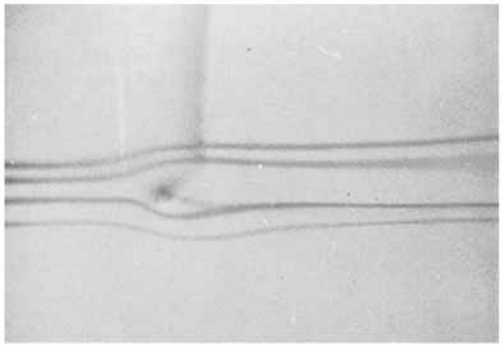

(*g*)

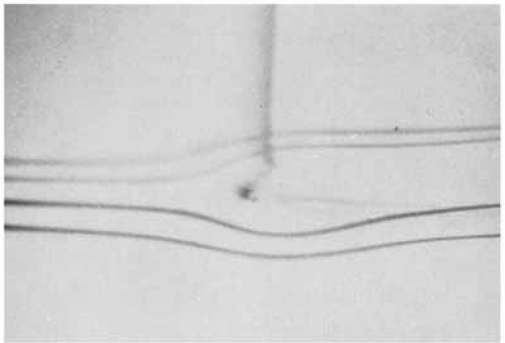

(*h*)

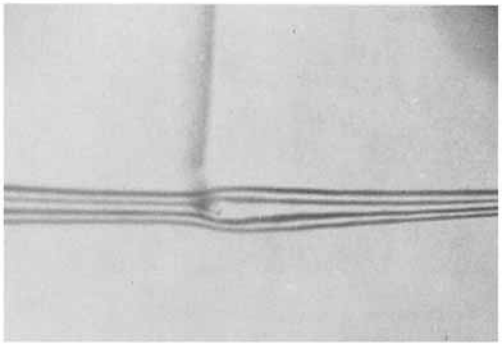

(*i*)

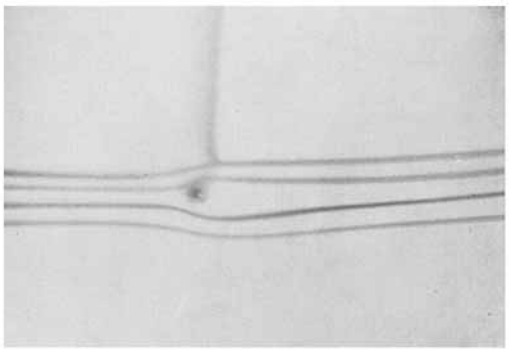

(*j*)

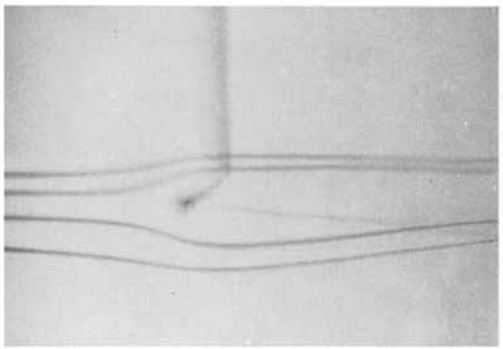

(*k*)

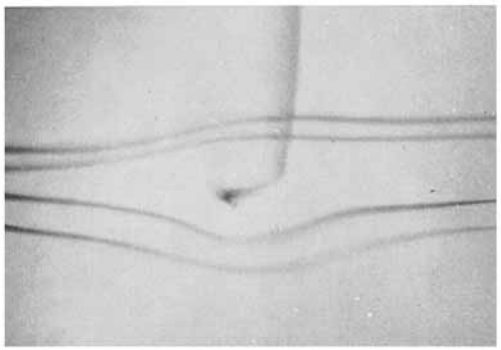

(*l*)

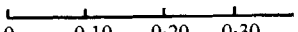

Concentration (ppmw)	Reynolds number 5	11	22	35
0	*a*	*b*	*c*	*d*
30	*e*	*f*	*g*	*h*
60	*i*	*j*	*k*	*l*

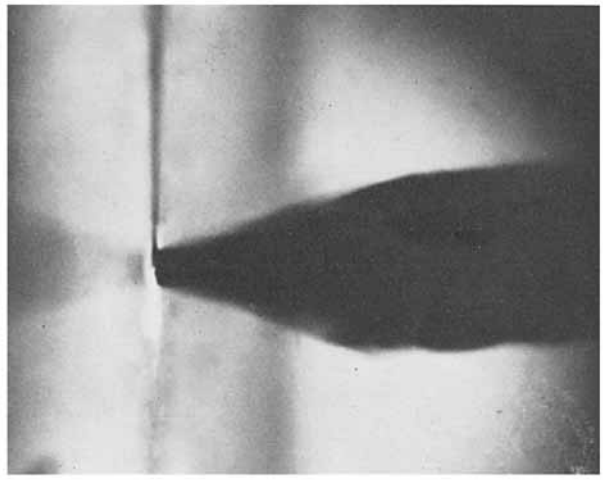

(*a*)

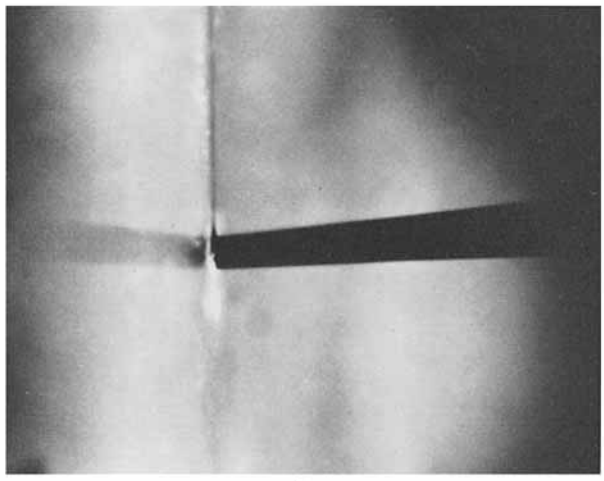

(*b*)

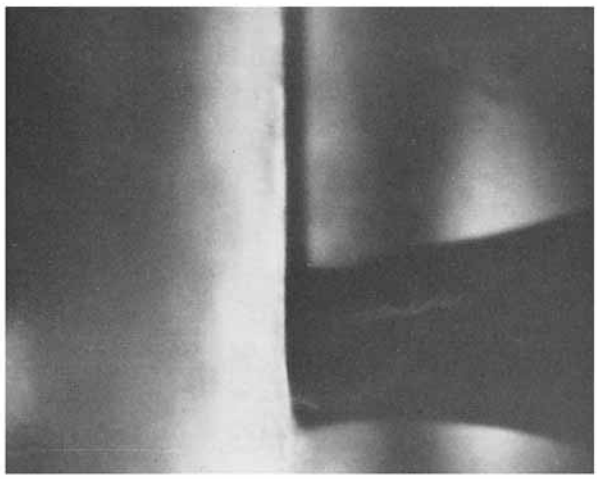

(*c*)

FIGURE 11. Photographs of a dyed liquid issuing from a 0·006 in. orifice into a water reservoir: (*a*) water at a mean velocity of 0·2 ft./sec; (*b*) water at a mean velocity of 1·5 ft./sec; (*c*) dilute polymer solution at mean velocity of 1·0 ft./sec.